Journal of
Marine Science and Engineering

MDPI

Article

Optimization of Combustion Cycle Energy Efficiency and Exhaust Gas Emissions of Marine Dual-Fuel Engine by Intensifying Ammonia Injection

Martynas Drazdauskas * and Sergejus Lebedevas

Faculty of Marine Technology and Natural Sciences, Klaipeda University, 91225 Klaipėda, Lithuania; sergejus.lebedevas@ku.lt
* Correspondence: medienabaldams@gmail.com

Abstract: The capability of operational marine diesel engines to adapt to renewable and low-carbon fuels is considered one of the most influential methods for decarbonizing maritime transport. In the medium and long term, ammonia is positively valued among renewable and low-carbon fuels in the marine transport sector because its chemical elemental composition does not contain carbon atoms which lead to the formation of CO_2 emissions during fuel combustion in the cylinder. However, there are number of problematic aspects to using ammonia in diesel engines (DE): in-tensive formation of GHG component N_2O; formation of toxic NO_x emissions; and unburnt toxic NH_3 slip to the exhaust system. The aim of this research was to evaluate the changes in combustion cycle parameters and exhaust gas emissions of a medium-speed Wartsila 6L46 marine diesel engine operating with ammonia, while optimizing ammonia injection intensity within the limits of P_{max}, T_{max}, and minimal engine structural changes. The high-pressure dual-fuel (HPDF) injection strategy for the D5/A95 dual-fuel ratio (5% diesel and 95% ammonia by energy value) was investigated within the liquid ammonia injection pressure range of 500 to 2000 bar at the identified optimal injection phases (A $-10°$ CAD and D $-3°$ CAD TDC). Increasing ammonia injection pressure from 500 bar (corresponding to diesel injection pressure) in the range of 800–2000 bar determines the single-phase heat release characteristic (HRC). Combustion duration decreases from 90° crank angle degrees (CAD) at D100 to 20–30° CAD, while indicative thermal efficiency (ITE) increases by ~4.6%. The physical cyclic deNO_x process of NO_x reduction was identified, and its efficiency was evaluated in relation to ammonia injection pressure by relating the dynamics of NO_x formation to local combustion temperature field structure. The optimal ammonia injection pressure was found to be 1000 bar, based on combustion cycle parameters (ITE, P_{max}, and T_{max}) and exhaust gas emissions (NO_x, NH_3, and GHG). GHG emissions in a CO_2 equivalent were reduced by 24% when ammonia injection pressure was increased from 500 bar to 1000 bar. For comparison, GHG emissions were also reduced by 45%, compared to the diesel combustion cycle.

Keywords: marine engine; ammonia; dual fuel; combustion cycle; HRC; combustion optimization; thermal efficiency; GHG emissions

check for updates

Citation: Drazdauskas, M.; Lebedevas, S. Optimization of Combustion Cycle Energy Efficiency and Exhaust Gas Emissions of Marine Dual-Fuel Engine by Intensifying Ammonia Injection. *J. Mar. Sci. Eng.* **2024**, *12*, 309. https://doi.org/10.3390/jmse12020309

Academic Editor: Leszek Chybowski

Received: 31 December 2023
Revised: 4 February 2024
Accepted: 7 February 2024
Published: 9 February 2024

Correction Statement: This article has been republished with a minor change. The change does not affect the scientific content of the article and further details are available within the backmatter of the website version of this article.

1. Introduction

In 2021, the maritime transport sector of the European Union accounted for 3–4% of all EU CO_2 emissions, which are one of the main components of greenhouse gas emissions [1]. To reduce CO_2, IMO purposefully introduced regulatory measures for newly built and operated ships [2,3]. In 2011, the Energy Efficiency Design Index (EEDI) was introduced for newly built ships, increasing energy efficiency through technological solutions while reducing emissions. Since 2023-01, ships in operation over 400 GT are indexed according to the Energy Efficiency Existing Ship Index (EEXI) and must meet the minimum requirements of the energy efficiency standard. Moreover, ships in operation over 5000 GT are obliged to collect and declare data of efficient energy use, and in case of insufficient energy efficiency assessment (CII), owners have to take corrective actions [3]. Addressing the climate change issue, IMO updated their GHG reduction strategy in 2023, and aim to reduce GHG emissions by 70–80% by 2040 compared to 2008 levels, and to reach zero GHG by 2050 [4]. In parallel, the EU has also set long-term targets for maritime transport to reduce GHG emissions by 90% by 2050 compared to 1990 levels according to SEC (2021) 562 directive [1]. To achieve the set targets, a significant reduction of CO_2 emissions in maritime transport sector is required, mainly by increasing energy efficiency use and using renewable and low-carbon fuel (hydrogen, ammonia). Logistic, hydrodynamic, and technological measures can potentially reduce GHG emissions from ships by 5–20% using renewable and low-carbon-dioxide-generating fuel—up to 100%, according to DNV [5]. In 2023-07, the EU adopted a regulation on additional measures related to the use of renewable and low-carbon fuels (FuelEU Maritime) [1]. The envisaged measures will ensure that the greenhouse gas intensity of the fuel used in the maritime transport sector gradually decreases over time from 2% in 2025 to 80% in 2050.

Different evaluations have found that existing IMO, EEDI, and EEXI (CII) measures are insufficient to achieve ambitious EU and IMO targets. It is expected that the use of zero or almost zero GHG technologies and fuel in international fleets will reach at least 5% by 2030, according to the 2023 IMO strategy plan [4]. The average operational age of ships in operation is 21.1 years in the economies of developed countries, and 28.6 years in the economies of developing countries [6]. Recently, on average, 79% of newly built ships annually choose traditional fuel, while 98.4% of ships in operation use petroleum fuel [7]. After evaluating the facts, it becomes obvious that the achievement of EU and IMO GHG reduction targets is related to retrofitting of newly built ships and operating ship power plants with renewable and low-carbon fuels such as ammonia.

Ammonia in shipping among renewable and low-carbon fuel species is assessed prospectively for the short-term 2025–2030 and the long-term 2050 period. Ammonia stores 50% more energy by volume than hydrogen [8], which is important considering limited fuel tank volume on board. Ammonia is also valued positively from a decarbonization perspective, as its chemical elemental composition does not contain carbon atoms which lead to the formation of CO_2 emissions when fuel is burned. However, there are a number of problematic aspects to using ammonia in maritime transport: due to nitrogen atoms in the chemical composition of ammonia, NO_x emissions are more intensively formed during combustion than compared to diesel [9]. In addition, a fraction of unburnt NH_3 emissions slip to the exhaust system during exhaust stroke. Ammonia emissions contribute to air pollution and can have detrimental effects on ecosystems, including acidification of soil and water bodies, which can harm plant and aquatic life. Moreover, ammonia emissions can lead to various human health issues. When individuals are exposed to elevated levels of ammonia over time or in concentrated forms, it can cause irritation and inflammation of the respiratory tract. Therefore, a solution to reduce these emissions is a priority in order to use ammonia in DE. Using ammonia in DE also requires solutions due to its unfavorable physical properties. In particular, ammonia combustion characteristics differ significantly from those of petroleum-based fuels and most renewable fuels (see Table 1). Due to a low fuel cetane number (5–7 units) and high auto-ignition temperature (650 °C), ammonia ignition is possible at an engine compression ratio of 35:1 and more, which is unrealistic to achieve considering the geometrical parameters of marine engines [10]. Therefore, to ensure ammonia combustion in diesel engines whose compression ratio usually reaches up to 20:1, pilot fuel with good auto-ignition characteristics is required (diesel, biodiesel).

Table 1. Comparison of fuel physical properties [9–11].

Fuel Property	Ammonia	Hydrogen	Methanol	LNG	Diesel
Formula	NH_3	H_2	CH_3OH	CH_4	$C_{12}H_{23}$
Density when liquified, kg/m^3	602.8	70.8	786.3	430	832
Calorific value, MJ/kg	18.8	120	19.7	38.1	42.7
Octane number	110	130	113	107	30
Cetane number	5–7	-	5–8	-	40–55
Ignition temperature, °C	651	585	385	540	254–285
Laminar flame speed, m/s	0.07–0.14	2.70	0.50	0.38	0.87
Stoichiometric air fuel ratio	6.06	34.32	6.45	17.2	14.5
Heat of vaporization, kJ/kg	1370	461	1103	510	232

Ammonia has a rapid and even kinetic combustion phase due to an efficiently mixed and evenly distributed ammonia and air mixture. On the other hand, it has more intense heat release compared to diesel, due to the kinetic ammonia combustion phase which leads to an increased maximum cyclic pressure (P_{max}). For example, with dual-fuel ratio D39/A61 (diesel 39% and ammonia 61%) [12], maximum cycle pressure reaches 86.2 bar when D100—76.3 bar. This has a negative impact on mechanical and thermal piston-rod group part loading, which reduces engine reliability. Reviewed studies in the literature are divided into two categories of dual ammonia diesel fuel injection into the cylinder: low-pressure dual-fuel strategy (LPDF), when ammonia in gaseous phase is introduced into the cylinder through the gas valve at low 2–3 bar pressure together with compressed air to intake manifold; and high-pressure dual-fuel strategy (HPDF), when ammonia in liquid phase is directly injected into the cylinder at high pressure through a separate fuel injector. Studies show that in both cases, engine ITE is close to that of a diesel engine, and with a fuel ratio of D20/A80 (diesel 20%, ammonia 80%) with LPDF strategy, ITE increases by 3.5% [13]. Nadimi et al. [12] have also found that higher engine ITE is achieved using ammonia, and that the difference in ITE compared to diesel engine mode is 17% (D100 (100% diesel) ITE—32%; D16/A84 ITE—37.6%). Indicative thermal efficiency increases when the engine is running on ammonia using LPDF strategy due to several reasons. According to the authors of [12], first of all, ammonia tends to have an ignition delay due to its high octane number and high autoignition temperature. Therefore, when transitioning to ammonia, an advanced start of diesel injection is necessary to achieve heat release characteristics similar to a diesel engine. Due to the advanced start of diesel injection, diesel has enough time to be evenly distributed in the combustion chamber. This results in a short and intense homogeneous heat release of the ammonia-diesel mixture. As a result, a lower combustion cycle temperature is achieved, leading to reduced heat losses through the cylinder walls to the cooling system. Heat loss decreased from 320 J/cycle when the engine was running only on diesel to 240 J/cycle at the fuel ratio A84/D16, when engine work did not change [12]. Also, less heat was lost through exhaust system as the exhaust gas temperature at the fuel ratio A84/D16 decreased by 132 °C compared to D100 [12]. Therefore, the distribution of the engine's heat balance components towards an increase in thermal efficiency is taking place. Aaron Reiter et al. [9] determined the highest ammonia diesel dual-fuel ratio at D5/A95 by energy value using LPDF strategy. However, engine fuel efficiency and ITE results under these conditions were very low, with ITE reaching 18.9%. Therefore, according to Aaron Reiter et al., this mode of engine operation is not rational. Nadimi et al. [12] used a wide range of ammonia ratios (0–84%) in a dual-fuel balance using LPDF strategy. However, at a higher percentage of ammonia, according to the authors, the engine lost its starting properties and did not start. Numerical studies by Tie Li and Xinyi Zhou et al. [13] also showed that at 90% ammonia in the dual-fuel balance, the combustion process became unstable when LPDF strategy was applied, and the mass fraction of unburnt NH_3 in the exhaust system increased more than six times. As a result, using LPDF strategy, the share of ammonia in the dual-fuel balance is limited to 80–84%. On the contrary, with HPDF strategy, the optimal proportion of ammonia in the dual-fuel balance is 95–97% [13,14]. In Tie Li and Xinyi Zhou et al., numerical studies [13] using HPDF strategy at the fuel ratio A97/D3 ITE practically did not change, and reached 45.3% while at D100—45.4%. Using LPDF strategy and the ratio, A80/D20 ITE reached 47.0% [13]. The increase of ITE is associated with lower heat losses to the cooling system due to the reduced interaction between the flame and cylinder walls close to top dead center (TDC) [13].

In addition to positive increase of ITE, GHG harmful components and CO_2 emissions are also higher with LPDF strategy. Using LPDF, more CO_2 emissions are released during the combustion cycle than compared to HPDF, as LPDF has a relatively large share of pilot fuel (diesel) in the dual-fuel balance ~20%. The amount of released CO_2 emissions during combustion depends solely on injected diesel mass [9,13]. It was also observed that N_2O, one of the GHG components, decreases in parallel with the increase of ammonia ratio in the dual-fuel balance. In the literature [12,15], it is hypothesized that during ammonia combustion, N_2O from the elemental chemical composition of ammonia is formed mainly in low-temperature zones during expansion stroke when NH_3 stuck in the gap between piston crown and cylinder liner turns into NH_2 and reacts with NO_2. This means that unburnt NH_3 and N_2O emissions correlate [15]. Numerical studies by Tie Li and Xinyi Zhou et al. [16] evaluated the differences between low and high dual-fuel injection strategies. NO_x emissions were found to be on average three times higher with LPDF than with HPDF strategy. Meanwhile, unburnt NH_3 emissions using HPDF injection strategy reached ~0.02 mg/kWh, while LPDF resulted 10–480 mg/kWh, depending on the fuel injection start angle. In continued numerical studies, Tie Li and Xinyi Zhou et al. [13], at fuel ratio A97/D3 using HPDF strategy, recorded NO_x emission levels approximately four times lower than at the fuel ratio A80/D20 with LPDF, and NH_3 emissions were also up to seven times lower. The reduction of NO_x emissions is associated with thermal deNO_x process of nitrogen oxides, during which active NH_2 radicals react with NO to form N_2 + OH at 1000–1400 K cylinder temperatures [17]. The reduction of NH_3 emissions is attributed to more efficient combustion characteristics due to liquid ammonia penetration to the pilot fuel spray flame zone [13]. As a result, HPDF compared to LPDF injection strategy does not make a significant difference in terms of ITE, but in terms of emissions, HPDF injection strategy emits less NH_3, NO_x, and CO_2 emissions in all cases. HPDF injection strategy also has the potential to reduce CO_2 and NO_x emissions compared to a diesel engine.

One of the important aspects of ongoing research is the arrangement of ammonia and diesel injector nozzle holes. The literature analysis shows that arrangement angle of diesel and ammonia nozzle holes has no significant effect on ITE, but ecological indicators differ. Tie Li and Xinyi Zhou et al. [16] found that, when ammonia and diesel fuel injector nozzle holes are overlapped (0° angle), a more efficient combustion process takes place. As a result, ammonia penetrates more efficiently into the pilot fuel combustion zone from the start of injection, and the induction period (from the start of injection till combustion) is shorter, and due to which the emission level of NO_x and NH_3 is lower. Meanwhile, ITE practically did not change and reached 51.6% when nozzle holes were overlapping, and 51.8% when nozzle holes were separated [16]. Valentin Scharl and Thomas Sattelmayer et al. [14], in their experimental studies of ammonia and diesel nozzle holes' arrangement influence on the induction period using HPDF injection strategy (2000 bar), also determined the optimal (0–7.5°) hole overlap range at which the shortest induction period and the most efficient fuel combustion, in terms of unburnt NH_3, were observed.

In summary, direct diesel engine transition to ammonia is limited due to ammonia's unfavorable physical characteristics, specifically, high exhaust gas emissions. Therefore, solutions to improve energy efficiency and reduce exhaust gas emissions while the engine is operating with ammonia is necessary. The optimization of the combustion cycle primarily involves adjusting fuel injection pressure, injection phase, and duration. The evolution of trends in modern diesel engines is grounded in numerous theoretical and experimental studies and justifications. Therefore, the systematic solutions they offer, including the identification of the main optimized parameters and their determining factors, are also rational in the case of ammonia use. Since the period of strategic thermal efficiency parameters increase for diesel engines, studies [18–21] have shown that under the condition P_{max} = const, heat release forming in the diesel engine cylinder practically does not affect ITE. The main factor influencing ITE is the heat release process duration. Based on these principles, the optimization of DE combustion cycle towards reducing the combustion duration primarily involves increasing fuel injection pressure. The increase in maximum combustion pressure is constrained by adjusting fuel injection timing towards TDC while simultaneously raising compression ratio. This approach was executed in MTU 396 series engines. Increased injection pressure was matched by adjusting the start of fuel injection to 4° CAD before TDC, and an increase in compression ratio (CR) from 15 to 17.8. Consequently, a 20% reduction in heat release duration was achieved, which resulted in improved fuel efficiency and NO_x reduction by 35% [21]. Thus, one of the most effective ways to influence heat release intensity is to increase fuel injection pressure. At the same time, increasing heat release intensity reduces combustion duration and increases combustion cycle dynamics and ITE. In parallel, adjusting the start of the injection angle closer to TDC, together with fuel injector design and parameters optimization, allows to improve ITE without the exceeded P_{max} limitation. Since the 1990s, a trend for optimizing the combustion process of market-leading diesel engines has emerged. During this period, studies were conducted on the influence of fuel injection pressure on fuel ignition and combustion dynamics [22–25]. Additionally, the ACE Company and the Japan Automotive Research Institute compared the effects of the duration and intensity of the initial fuel injection stage on air swirl parameters. Furthermore, comprehensive improvements were made to exhaust gas toxicity indicators by companies such as MTU, YaMZ, and Fev Motorentechnik GmbH & Co., KG [22,24,26].

The application of combustion cycle optimization trends, such as advancing the start of pilot fuel injection, changing injection rate and pressure, and organizing multistage injection, have enabled market-leading companies (Wärtsilä, MAN B&W, Caterpillar, etc.) to develop dual-fuel engines with LNG. These advancements have allowed them to achieve thermal efficiency similar to diesel engines and reduce PM and NO_x emissions by up to 90% compared to diesel engines [27–29]. Therefore, to increase ITE and reduce emissions by optimizing combustion cycle parameters, this research is based on fuel injection intensification by increasing injection pressure.

Considering the wide variety of diesel engines and models of ship power plants in operation, it is rational to base marine transport sector decarbonization with engine retrofitting based on numerical studies to reduce time and financial costs. Engine retrofitting for operation with other types of fuel by numerical methods is basically related to research and optimization of combustion cycle characteristics. Numerical research tasks for the ship's main propulsion diesel engine's operation on ammonia fuel are based on multizone mathematical models (MM), for example, using simulation software "AVL FIRE M". The use of multi-zone MM allows us to study combustion cycle physical processes with sufficient accuracy for solving practical problems. Klaipeda University conducted comprehensive marine diesel engine decarbonization research, including solutions for the rational use of renewable and low-carbon fuels [30–32], the use of secondary heat sources in engine cogeneration cycle [33], etc.

In this article, the research of ammonia combustion was performed to identify physical combustion process conditions and to provide rational technological solutions for ammonia applicability in ship power plants. The novelty of this article lies in the organization of combustion process. Marine engines operate under different conditions compared to automotive engines. One significant difference is in how the fuel interacts with the engine components. Unlike automotive engines, where the fuel film along the cylinder walls is common, marine engines are designed to avoid direct contact between the fuel jet and the cylinder walls. This difference in design and operation significantly alters the combustion characteristics of marine engines. Therefore, the purpose of this article is to evaluate the changes in combustion cycle parameters and exhaust gas emissions for the ship's propulsion diesel engine operating on ammonia, and to determine the limits of combustion cycle regulation parameters (NH_3 injection intensity when increasing the injection pressure). At the time of writing, the authors are not aware of any similar published articles, making this approach unique in optimizing the ammonia combustion cycle. The presented research approach could provide valuable insights for combustion cycle optimization during the transition of marine diesel engines to ammonia, requiring minimal changes to the engine structure. In addition, the NH_3 combustion cycle optimization strategy by injection intensification is related to optimization of the pilot diesel and ammonia injection phases, and is planned for continuous studies.

2. Materials and Methods

2.1. Research Object

A marine medium-speed four-stroke Wartsila 6L46 diesel engine (Wartsila: Helsinki, Finland) was selected as the research object. Medium-speed (300–1000 rpm) four-stroke diesel engines are widespread in ship propulsion systems, especially in smaller cargo ships, as well as in larger specialized ships, such as cruise ships, ferries, and ro-ro cargo ships [34]. Medium-speed four-stroke diesel engines' popularity is due to their higher power-to-weight and power-to-space ratio, easier periodic maintenance, and acquisition costs compared to low-speed two-stroke diesel engines [35]. Market-leading engine manufacturers' (BERGEN, WARTSILA, MAN) medium-speed four-stroke diesel engines thermal efficiency reach 46–49% when emission level meets IMO Tier II regulation, while using SCR technology meets IMO Tier III [36–38]. Research object selection and simulation model verification were carried out according to real DE data obtained during operation to bring research results as close as possible to practical application for maritime transport decarbonization. Table 2 presents the main research object structural parameters.

Table 2. Wartsila 6L46 engine data.

Parameter	Data
Bore, mm	460
Stroke, mm	580
Connecting rod length, mm	650
Compression ratio	12.5
Engine speed, rpm	500
Compressed air pressure at inlet valve close, bar	3.45
Compressed air temperature at inlet valve close, K	372
Inlet valve closing angle, CAD	120° BTDC
Exhaust valve closing angle, CAD	128° ATDC
The total number of injection holes for ammonia and diesel injectors	10
The location of ammonia and diesel injectors	Centre
Piston surface type	Bowl-In Piston

2.2. Research Strategy

Guidelines for the Wartsila 6L46 engine model creation to run on ammonia for numerical studies using AVL FIRE M simulation software (version 2022 R2) is based on findings of conducted research in the literature. Due to lower concentrations of NO_x and NH_3 emissions during combustion cycle, ammonia fuel injection is organized in liquid phase. Due to greater CO_2 emission reduction effect, the selected dual-fuel ratio of diesel and ammonia is D5/A95 (5% diesel and 95% ammonia according to energy value). To ensure the shortest induction period and the most effective combustion, the diesel and ammonia injectors' nozzle holes are overlapped (0° angle). Simulations were performed with the same amount of heat input. Inlet air pressure and temperature were unchanged for D100 and D5/A95. Initial simulation data are presented in Table 3.

Table 3. Initial data used for simulation.

Parameter	Diesel (D100)	Ammonia + Diesel (D5/A95)
Start of injection, CAD	710°	710 NH_3; 717 Pilot
Diesel injection duration, CAD	26°	3
Ammonia injection duration, CAD	-	26°
Injected mass (Diesel), g	1.87	0.1037
Injected mass (Ammonia), g	-	4.016
Injection pressure (Diesel), bar	500	500
Injection pressure (Ammonia), bar	-	500–2000
Diesel calorific value, MJ/kg	42.5	
Ammonia calorific value, MJ/kg	18.8	

2.3. Mathematical Model and Verification

Numerical mathematical studies of combustion cycle characteristics were performed by transferring a ship's propulsion main diesel engine Wartsila 6L46 (B/S = 460/580 mm, 500 rpm, 4 stroke, 6 cylinders, 6300 kW) to ammonia operation. Engine combustion chamber mesh for simulation was created using "AVL FIRE ESE DIESEL" software (version 2021 R1). To reduce simulation time, it was decided to perform the simulation for 1/5 part of the total combustion chamber (360°/5 = 72). Despite the fact that the simulation was performed on a 1/5 combustion chamber, emission results are presented for a full engine, i.e., six cylinders. Total fuel injection nozzle quantity for full chamber is 10; therefore, for 1/5 part, the injection nozzle quantity was set to 2. Injected ammonia and diesel mass was reduced to 1/5 part. The diesel and ammonia injection nozzles spray cones are overlapped, meaning 0° angle distribution. An example of nozzle distribution is presented in Figure 1a. The total number of cells was 97,076, average cell size was 3.80 mm, number of boundary layers was 2, thickness of boundary layers was 0.60 mm, and number of subdivisions in angular direction was 50 (Figure 1b).

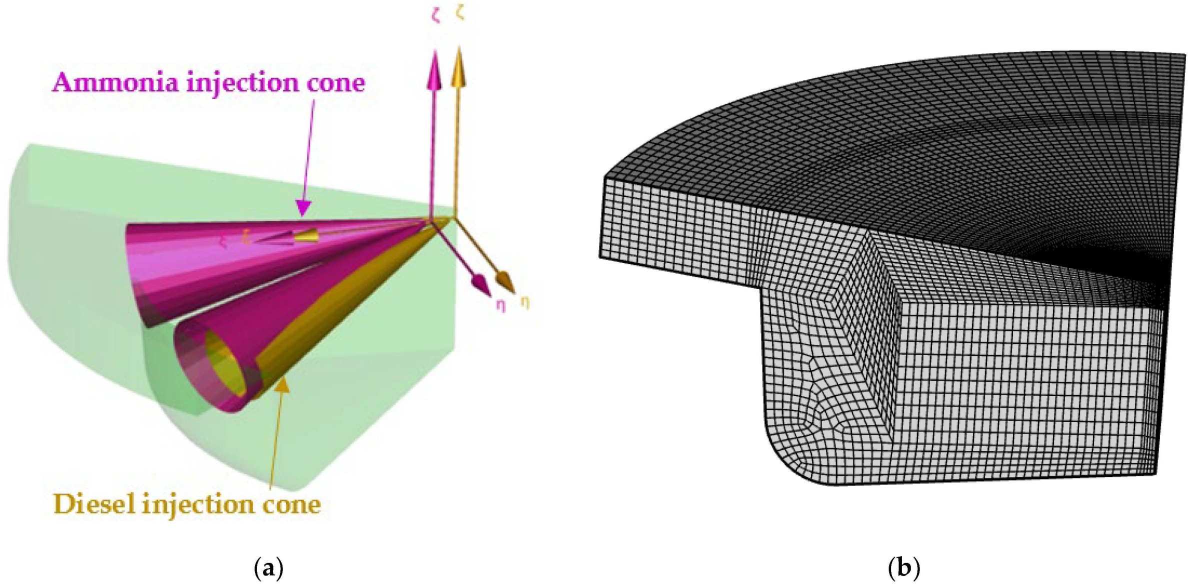

Figure 1. (**a**) Injector nozzle hole arrangement (0° angle) inside combustion chamber sector (pink—NH_3, gold—diesel); (**b**) 1/5 (72°) combustion chamber sector mesh.

Numerical studies were conducted using the multi-zone mathematical model developed by AVL company, specifically designed to investigate the physical processes involved in the ammonia combustion cycle. The gas phase reaction model, combining combustion and emission models, is capable of solving diesel and ammonia combustion reactions. General gas phase reaction model includes H, O, C, N, HE, and AR chemical elements and 54 numbers of species. The model is based on P. Glarborg's methodology for modeling nitrogen chemistry in combustion [39]. The experimental verification of the model was conducted by AVL company. Since combustion model is not yet commercially publicly available by AVL decision, the description of the general gas phase reaction model is not provided.

The spray module for calculating droplets in the simulation region uses the Lagrangian approach [40]. The droplets are tracked in a Lagrangian way through the computational grid used for solving the gas phase partial differential equations. Additional spray submodels, such as the the Schiller–Naumann injection drag model [41] and Abramzon–Sirignano evaporation model [42], were selected for this simulation.

AVL FIRE M simulation software focuses on detailed analysis of physico-chemical processes taking place in the cylinder. However, it does not provide the combustion cycle (IMEP, BSFC, P_i, ITE) parameters. Therefore, these parameters are calculated from the array of AVL FIRE M simulation results according to given formulas.

Indicated mean effective pressure, IMEP, is calculated according to trapezoidal approximation Formula (1) [43]:

$$\mathrm{IMEP} = \frac{1}{\mathrm{V_{cyl}}} \sum_{k=\theta_0}^{\theta_f} \frac{\mathrm{P_{k+1}} + \mathrm{P_k}}{2} \cdot (\mathrm{V_{k+1}} - \mathrm{V_k}) \tag{1}$$

where V_{cyl} is cylinder volume [m^3]; P_k and P_{k+1} are consecutive cylinder pressure readings [bar]; V_k and V_{k+1} are cylinder volume measurements corresponding to P_k and P_{k+1} [m^3]; and the sum in increments of k from a crank angle degree value θ_0 to a value θ_f are calculated.

Indicated power P_i is calculated as per below Formula (2) [44]:

$$\mathrm{P_i} = \frac{\mathrm{IMEP} \cdot \mathrm{V_{cyl}} \cdot \mathrm{n} \cdot \mathrm{N}}{\mathrm{z} \cdot 60} \tag{2}$$

where n is cylinders number; N is engine speed [rpm]; and z is coefficient (z = 1 for 2-stroke engines, z = 2 for 4-stroke engines).

Specific fuel consumption, BSFC, is calculated according to the presented Formula (3) [44]:

$$\mathrm{BSFC} = \frac{\mathrm{m_f}}{\mathrm{P_i}} \tag{3}$$

where m_f is fuel consumption [kg/h].

Engine indicative thermal efficiency, ITE, is calculated as per the below Formula (4) [44]:

$$\mathrm{ITE} = \frac{3600 \cdot \mathrm{P_i}}{\mathrm{m_f} \cdot \mathrm{H_u}} \tag{4}$$

where H_u is calorific value of kilogram fuel [kJ/kg].

An indicator diagram was measured for all six cylinders and averaged when the engine was running on D100 at 75% load. The combustion cycle parameters (IMEP, BSFC, P_i, P_{max}, ITE) were calculated from the indicator diagram using Formulas (1)–(4). The Wartsila 6L46 simulation model was created using AVL FIRE M simulation software. The simulation was performed when the engine was running on D100 at 75% load for model verification. A simulation indicator diagram was matched with the real operating engine indicator diagram for the combustion cycle from -120° (intake valve closing, corresponding to 600° in the software) to +128° (exhaust valve opening, corresponding to 848° in the software) crankshaft rotation angles when TDC was at 720° (Figure 2). The error of simulation meant indicative pressure compared to real engine value reached 2.4%. Indicator combustion cycle thermodynamic temperature and emission (CO_2, N_2O, CH_4, NO_x, NH_3) diagrams were calculated in parallel. A verified diesel engine combustion cycle simulation model was considered as the base engine operating mode for this research, and will be used for further comparison.

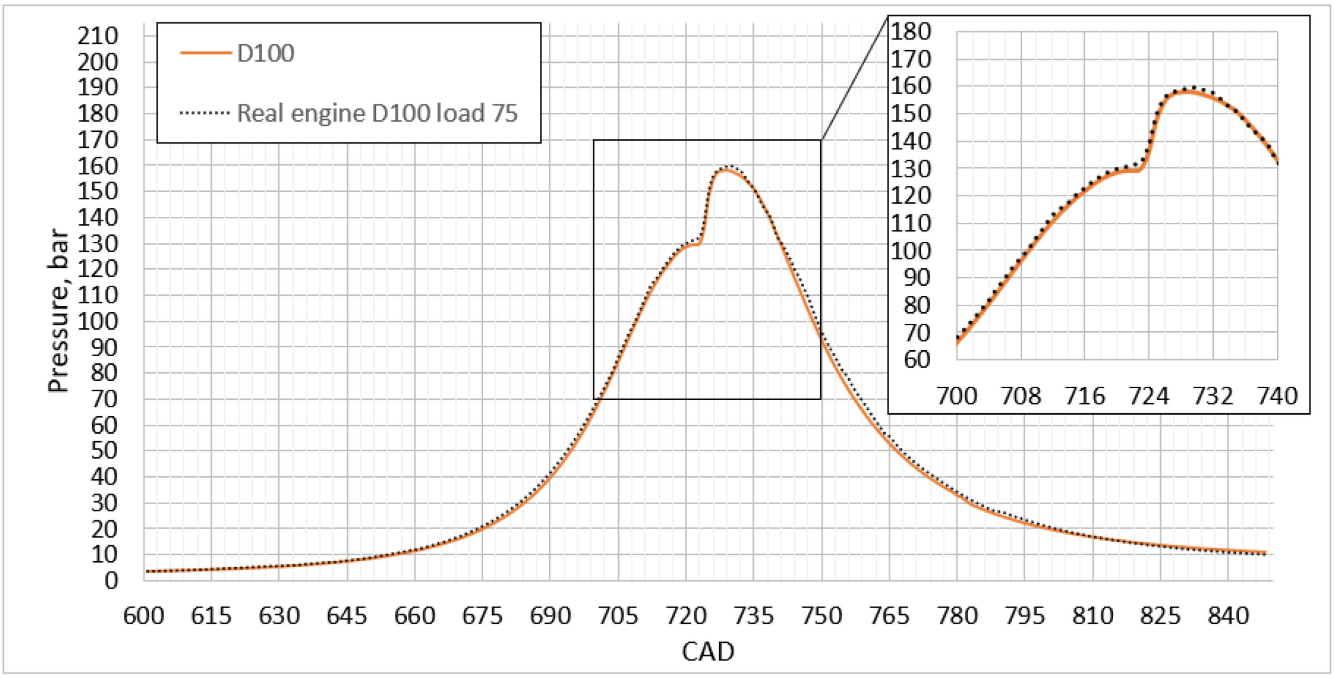

Figure 2. Verification of simulation indicator diagram with real operating engine indicator diagram.

Ammonia combustion and emission model validation through experiment was not feasible on operating the marine diesel engine. Therefore, the model validation relies on similar simulation results found in the literature [13,16]. In the literature, studies primarily focus on examining ammonia utilization technologies for relatively small cylinder diameter high-speed engines for automotive applications, with the exception of [16]. There is a notable absence of information regarding the application of ammonia to medium- and low-speed marine engines, despite ammonia being regarded as one of the primary alternative fuels in this sector. To justify the verification of the mathematical model, a comparative analysis of obtained results was performed with two articles which were discovered in the literature involving diesel engines running on ammonia using HPDF strategy and a similar dual-fuel ratio alongside ammonia injection pressure. A direct comparison of the combustion cycle parameters and exhaust gas emissions of this research to the literature would provide inaccurate results due to differences in engine types and combustion cycle organization. Thus, a comparison in the relative change in parameters compared to the diesel combustion cycle was selected. A detailed comparison of these parameters is provided in Table 4. In Case 1, ammonia injection pressure is set at 500 bar for the presented simulation results and 600 bar for simulation results in the literature [13], while Case 2 involves a 1000 bar ammonia injection pressure for both the present and the literature results [16]. Despite differences in engine speed and fuel start of injection angles, ammonia combustion in both cases resulted in a similar ignition delay. Moreover, the heat release rate matches with the literature as it progresses towards the expansion stroke in a similar manner. P_{max} also exhibits good agreement with the literature at 500 and 1000 bar ammonia injection pressures. For example, for Case 1 P_{max} decreases by 17% and 8%, while for Case 2, it increases by 9% and 10%. T_{max} mostly corresponds to the literature, while thermodynamic temperature (T) at 60° CAD after TDC shows a decreasing trend. Furthermore, exhaust gas emissions correspond to the literature in the same direction. In conclusion, ammonia combustion and emission model provide similar relative changes in combustion cycle parameters and exhaust gas emissions compared to the literature.

Table 4. Comparison of dual ammonia–diesel fuel combustion cycle research results with results from the literature review [13,16].

	Case 1		Case 2	
Parameter	**P_{inj} 500 bar**	**Li, T. et al. [13]**	**P_{inj} 1000 bar**	**Li, T. et al. [16]**
Engine type	4-stroke	4-stroke	4-stroke	2-stroke
Bore, mm	460	95	460	340
Stroke, mm	580	102	580	1600
Engine speed, RPM	500	1000	500	157
Dual-fuel ratio	D5/A95	D3/A97	D5/A95	D3/A97
Diesel injector nozzle hole number	10	8	10	4
Ammonia injector nozzle hole number	10	8	10	4
Diesel and ammonia injector nozzle hole angle	0°	0°	0°	0°
Diesel injection pressure, bar	500	600	500	200
Ammonia injection pressure, bar	500	600	1000	1000
Start of diesel injection, CAD	−3° TDC	−8° TDC	−3° TDC	−4° TDC
Start of ammonia injection, CAD	−10° TDC	−5° TDC	−10° TDC	−2° TDC
Ammonia ignition delay after diesel ignition, CAD	7°	4°	4°	1°
* P_{max}, %	>17	>8	<9	<10
* T_{max}, %	>2	>7	<10	0
* T at 60° CAD ATDC, %	>5	>7	>7	>20
* ITE, %	<2.2	0	<4.6	>1.1
* CO_2, %	>94	>96	>94	>96
* NO_x, %	>72	>50	>5	>46
N_2O, g/kWh	from 0.003 to 1.67	from 0 to 25 ppm	from 0.003 to 1.22	from 0.0007 to 0.0016
Unburned NH_3, g/kWh	from 0.011 to 8.94	from 0 to 130 ppm	from 0.011 to 1.51	N/A

* Relative change in parameters compared to diesel (D100) combustion cycle results. Symbol '<' refers to increase and '>' refers to decrease. N/A: value was too small to determine.

3. Results

3.1. Combustion Cycle Parameters

Several studies with ammonia used in DE are associated with poor combustion characteristics and therefore high emissions of unburnt NH_3 [9,10,12,13,15,16]. Ammonia injection pressure ranges of 500–2000 bar are chosen for numerical studies to improve combustion characteristics and evaluate the dependence of harmful substances on fuel injection pressure. In this case, the start of injection for ammonia is constant at 710° CAD, while for pilot diesel it is 717° CAD (720° = TDC). Result analysis shows (see Figure 3) that diesel induction period is 4° CAD (observed from start of fuel injection until the first visible increase in heat release). Meanwhile, the ammonia induction period (represented by the second peak) lasts 13°, 14°, 15°, 16°, and 18° CAD at 2000, 1500, 1000, 800, and 500 bar, respectively. Increasing ammonia injection pressure shortens the induction period during which fuel is mixed with air and vaporized. When evaluating the induction period, it is useful to separate the diesel combustion and subsequent ammonia combustion, as the latter leads to a delay in the heat release characteristic. At injection pressures of 2000–800 bar, ammonia combustion delay after ignition of pilot fuel at 721° CAD is 2–5° CAD, while at 500 bar the delay reaches 7° CAD. In this case, a significant difference in combustion phases was determined from the differential heat release characteristic due to a delay in ammonia ignition. The first increase in heat release rate chart (Figure 3), especially at 500 bar ammonia injection pressure, is associated with the diesel combustion phase, and the second one with ammonia. As a result, the heat release characteristic became double phase. Delayed ignition of ammonia also leads to structural changes of the combustion cycle parameters and exhaust gas emissions. The primary increase in P_{max} resulting from the increase in ammonia injection pressure is fundamentally related to structural changes in the ammonia jet. Specifically, the fineness and uniformity of ammonia droplets increase [45,46]. Consequently, the evaporation time of the droplets is shorter, leading to a reduction in the induction period. Additionally, due to the uniformity of the droplets in the jet (i.e., a narrower range of differences in droplet diameters), when the flame covers a large volume of the jet, it triggers a much more intense heat release. On the other hand, a shorter induction period advances the ammonia combustion start phase to earlier angles, while maintaining the same diesel ignition phase (Figure 3). As a result, before the phase change of P_{max} at ~720° CAD, the amount of heat released after TDC, which determines P_{max} and corresponding T_{max} values, increases intensively. As a result (Figure 4), using ammonia in DE increases maximum cyclic temperature (T_{max}) in all cases. An increase in maximum cyclic pressure and temperature has a negative impact on the mechanical and thermal loading of the piston-rod group and, as a result, on engine reliability. Therefore, P_{max} and T_{max} are limited to research object design P_{max}—160 bar and T_{max}—1566 K, considering the D100 combustion cycle parameters. In the presented indicator diagram (Figure 5), P_{max} increases to 194 bar at 2000 bar injection pressure, but decreases to 132 bar at 500 bar pressure. Correspondingly, at 2000 bar injection pressure in the thermodynamic cycle temperature chart (Figure 4), T_{max} reaches 1779 K, while at 500 bar—1540 K. A summary evaluation of P_{max}, T_{max} and ITE parameters in relation to ammonia injection pressure and D100 cycle is shown in Figure 6.

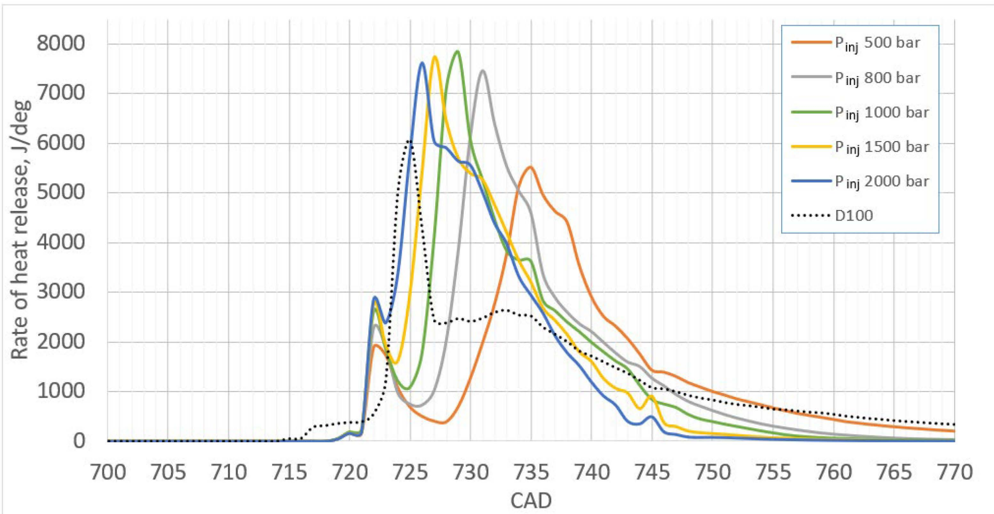

Figure 3. Heat release rate of ammonia injection pressure variations.

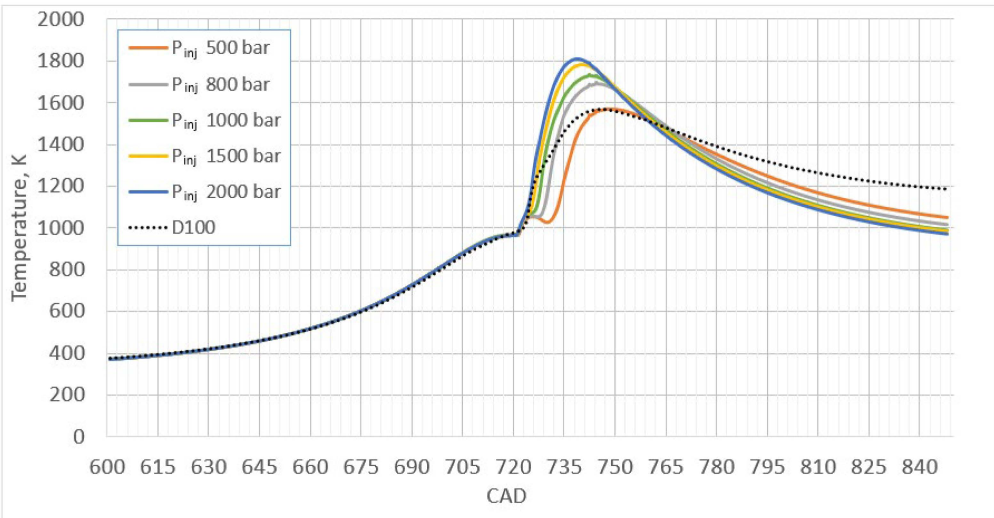

Figure 4. Temperature diagram of ammonia injection pressure variations.

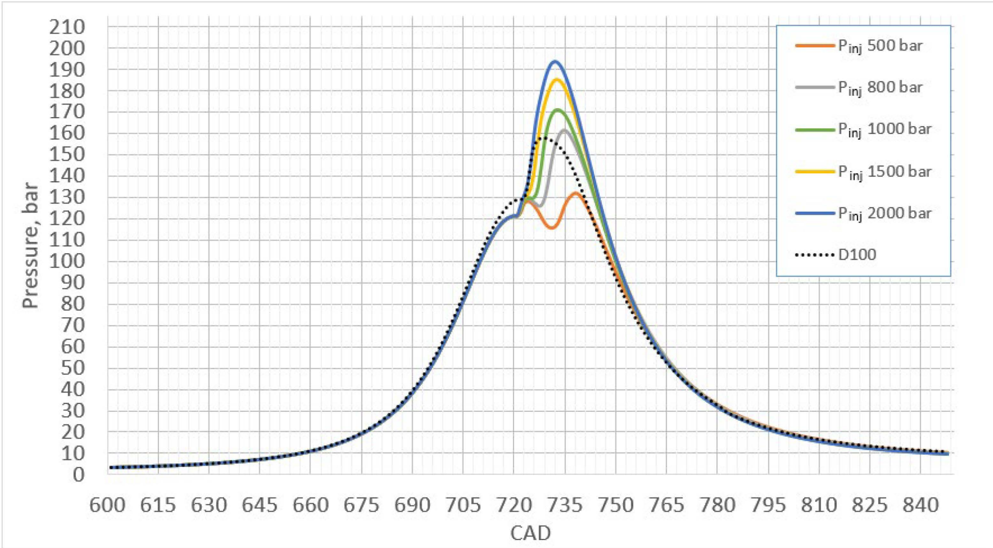

Figure 5. Indicator diagram of ammonia injection pressure variations.

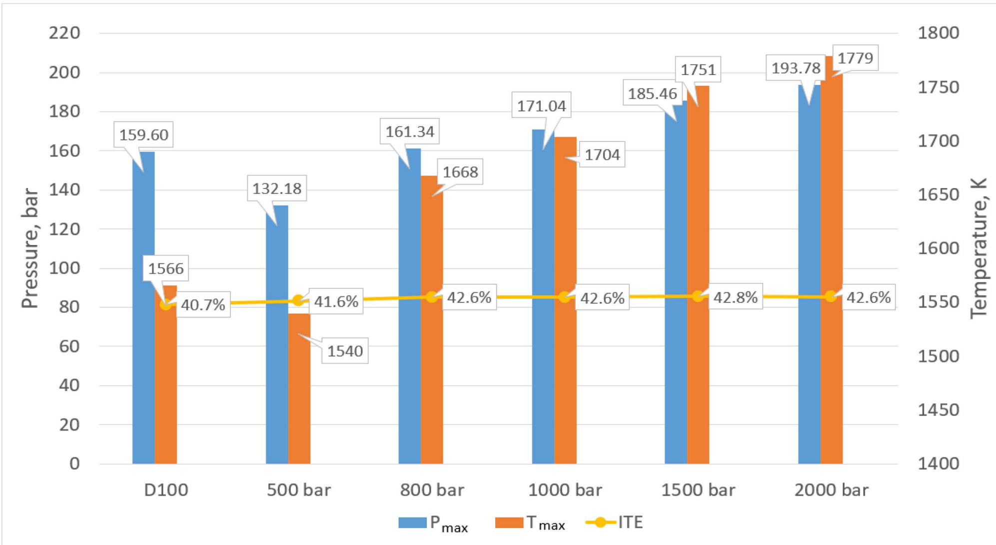

Figure 6. Comparison of P_{max}, T_{max}, and ITE variations of ammonia injection pressure with D100.

When comparing combustion cycle results at various ammonia injection pressures, it was found that ammonia injection pressure has no significant effect on indicative thermal efficiency. Only at 500 bar injection pressure is there a noticeable difference. Achieved ITE is 2.4% lower than at the remaining injection pressures. The reason was the delayed combustion in expansion stroke, at which the cylinder wall area increased and, accordingly, the heat loss to the cooling system increased. This can be validated by evaluating the integral of heat release (Figure 7). At 500 bar ammonia injection pressure, combustion duration reached ~60° CAD according to 95% of total heat release introduced with the fuel (corresponding to the limit of 75,000 J). The decrease in ITE was also influenced by a decrease in P_{max} and T_{max}, which determined the low combustion efficiency, which is determined by increase of unburnt NH_3 emissions. As a result, it was found that part of the heat introduced with the fuel was not released by evaluating the integral of heat release characteristic results at the end of the cycle. Meanwhile, gradually increasing the injection pressure above 800 bar results in a short combustion duration of 20–30° CAD, while at D100, combustion duration is ~90° CAD. Therefore, gradually increasing the ammonia injection pressure above 800 bar resulted in a high ITE of 42.6–42.8%, when D100 reached only 40.7%. In a general assessment, when the test engine was transferred to dual-fuel operation with ammonia, a 4.6% increase in ITE compared to the D100 combustion cycle was determined. The ITE increase coincides with other authors' results [9,12,13]. The increase in ITE is associated with a short and intense heat release close to TDC, due to which heat losses through the cylinder walls are lower.

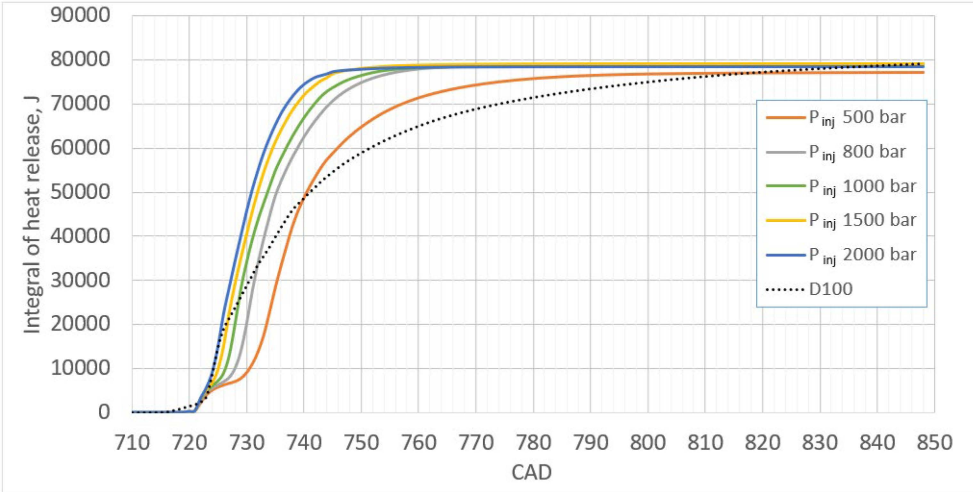

Figure 7. Integral of heat release of ammonia injection pressure variations.

To conclude, it can be stated that when optimizing ammonia and pilot fuel injection pressure, it is necessary to achieve a short combustion, and, respectively, a single-phase heat release, which is ensured by a short induction period. In this way, high ITE and combustion efficiency are achieved. However, increasing injection pressure also increases P_{max} and T_{max}, which are limited to research engine design data.

3.2. Ecological Indicators

Analyzing the release of harmful substances at the end of the combustion cycle, it was confirmed that CO_2 does not depend on injection pressure, since ammonia does not have carbon atoms in its chemical composition, so the release of CO_2 is mainly from injected pilot diesel mass. As a result, at 5% diesel mass by energy value, CO_2 emissions decreased up to 17 times and reached 33 g/kWh, when D100—564 g/kWh. CH_4 emissions, which also depend on pilot diesel mass, are estimated to have a 29.8 times greater contribution to the greenhouse effect than CO_2. During the ammonia combustion cycle, CH_4 decreased from 4.01 g/kWh to 0.00249 g/kWh at 500 bar and to 0.00023 g/kWh at 2000 bar. In this case, ammonia injection pressure has a significant influence on CH_4, since CH_4 as an incomplete combustion product depends on combustion efficiency.

In contrast to the decrease of CO_2 and CH_4 emissions, the N_2O component of GHG, which is estimated to have 273 times greater contribution to greenhouse effect than CO_2, is increasing. Published studies show that the N_2O formation mechanism during ammonia combustion takes place at temperature lower than 1400 K [12]. During combustion, NO and NO_2 react with NH and NH_2 radicals to form N_2O according to chemical reactions (5) and (6):

$$NH + NO \rightarrow N_2O + H \tag{5}$$

$$NH_2 + NO_2 \rightarrow N_2O + H \tag{6}$$

As a result, N_2O directly depends on combustion chamber temperature and ammonia fuel mass. This resulted in N_2O emissions of 1.67 g/kWh at lower combustion chamber temperatures at 500 bar injection pressure and 0.59 g/kWh at 2000 bar, with D100 at just 0.003 g/kWh. N_2O formation is analyzed by comparing visual results of N_2O mass fraction distribution in the combustion chamber with temperature fields at 770° CAD (Figure 8). Visual results analysis shows that N_2O is formed around the ammonia flame field only in 1000–1400 K temperature zone, while no N_2O formation was observed outside this temperature zone. Therefore, changing the ammonia injection pressure, which affects combustion temperature, can change the amount of N_2O emissions at the end of the combustion cycle. After comparing N_2O mass fraction distribution in the combustion chamber (Figure 8) at 500, 1000, and 2000 bar injection pressure, it was found that, in all cases with a similar temperature field around the flame field, the intensity of N_2O mass fraction distribution differs. At 1000 and 2000 bar, the intensity of N_2O mass fraction distribution is obviously lower, which can be attributed to unburnt NH_3 mass fraction distribution. NH_3 mass fraction in studied areas at 1000 and 2000 bar injection pressure is also lower due to more effective combustion. It can be reasonably stated that N_2O formation depends not only on temperature, but also is inseparable from ammonia fuel concentration in the combustion chamber.

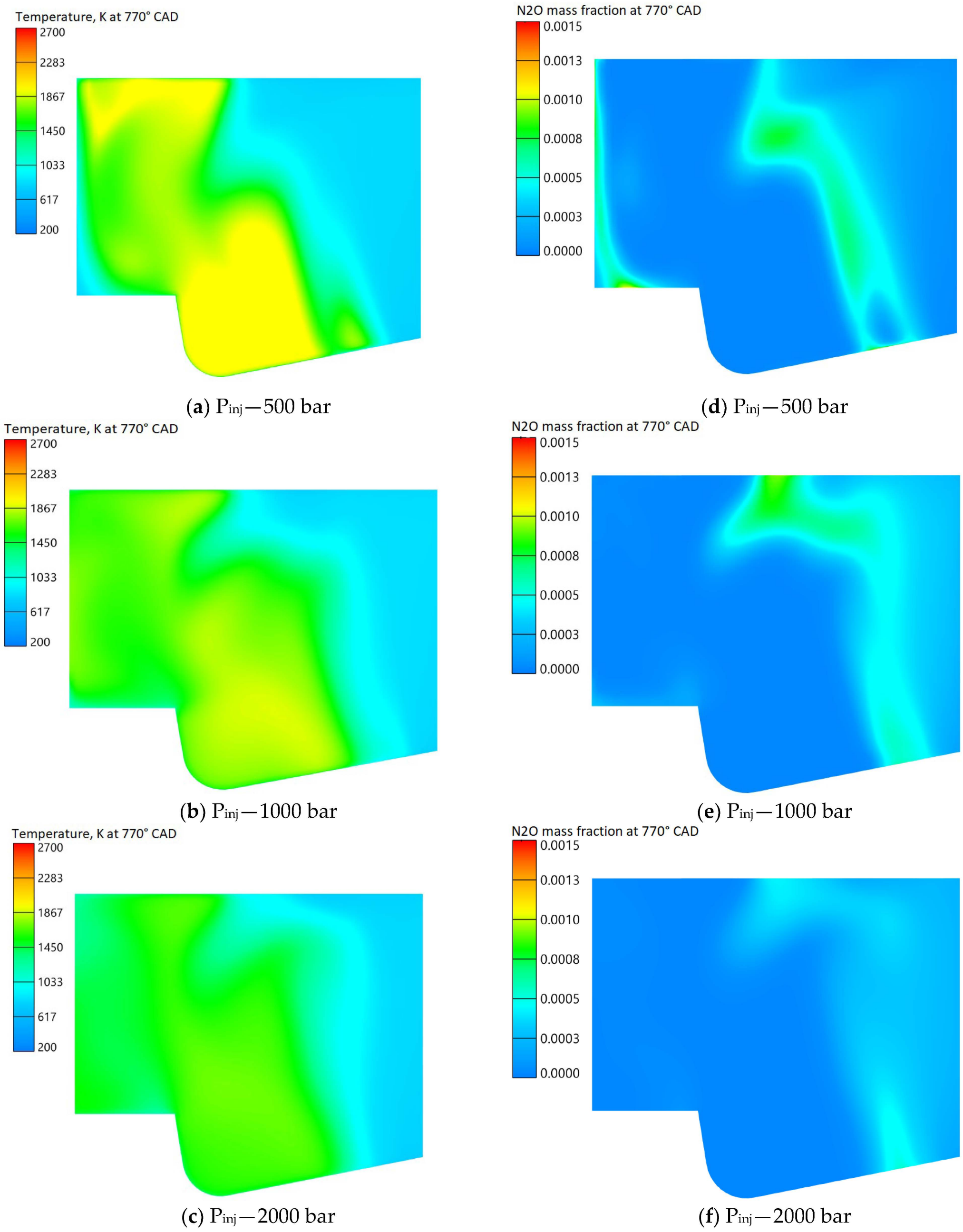

Figure 8. Comparison of N_2O cyclic mass fraction in combustion chamber with temperature fields at 770° CAD at 500, 1000, and 2000 bar ammonia injection pressure. (**a**–**c**) Temperature; (**d**–**f**) N_2O mass fraction.

On the other hand, NO_x emissions formation, which are also partially dependent on N atoms amount in fuel mixture, is also inseparable from injected ammonia mass. However, NO_x also depends on the combustion chamber temperature. Usually, thermal NO_x is formed at a combustion chamber temperature higher than 1600–1700 K, and with the increasing temperature, especially up to 2000 K and above [17,47], NO_x concentration increases exponentially. As a result, the highest amount of NO_x (9.42 g/kWh) were observed at the highest combustion temperature (T_{max}—1779 K) at 2000 bar injection pressure, while at 500 bar (T_{max}—1540 K) NO_x was lower (1.32 g/kWh). However, thermodynamic temperature reveals NO_x formation conditions quite conditionally; therefore, further evaluation of NO_x formation is carried out in relation to the structure of the combustion chamber local temperature field. Visual analysis of NO_x mass fraction distribution in the combustion chamber compared to temperature fields at 735° and 745° CAD (Figure 9) perfectly reflects thermal NO_x formation conditions. It was observed that the largest part of NO_x mass is emitted precisely in the highest temperature zones. However, observed insignificant NO_x mass fraction formation zones below 1700K combustion chamber temperature indicate fuel bound NO_x emissions. Therefore, at 500 bar ammonia injection pressure with smaller high temperature areas, NO_x formation was reasonably lower compared to 1000 or 2000 bar injection pressure. An interesting result was also observed, that despite high concentration of N atoms in dual-fuel balance, NO_x was formed 3.6 times less at 500 bar ammonia injection pressure than at D100, at practically the same maximum temperatures (D100 T_{max}—1566 K, D5/A95 500 bar T_{max}—1540 K). This phenomenon can be explained by the deNOx process, when at the cylinder temperature in range of 1000–1400 K, active NH_2 radicals react with NO to form N_2 + OH [17]. This process can be observed in the chart of NO_x cyclic mass fraction dependence on CAD (Figure 10). During heat release, NO_x emissions increase exponentially, peaking at the highest combustion chamber temperature. However, as temperature decreases, NO_x also begins to decrease due to the above chemical reaction. It was found that when ammonia injection pressure is 500 bar and T_{max} reaches 1540 K, the deNO_x process is three times more intense compared to 2000 bar and T_{max} 1779 K. This is because, at 500 bar injection pressure, the open temperature window duration of 1000–1400 K is longer.

Unburnt NH_3 that slip into that exhaust system also raises concerns in the scientific community for large scale use of ammonia in DE due to ammonia toxicity to living organisms. Emissions of unburnt ammonia indicate combustion efficiency. NH_3 emissions were found to be dependent on ammonia injection pressure. At lower injection pressure, a strong increase in unburnt NH_3 was recorded, which is related to relatively poor ammonia vaporization in the combustion chamber volume. The visual results of NH_3 mass fraction distribution in the combustion chamber at 770° CAD (Figure 11) show that, at 500 bar injection pressure, burnt ammonia areas (blue color) are uneven and do not cover most of the combustion chamber area compared to NH_3 results at 2000 bar injection pressure. At 500 bar injection pressure, the level of NH_3 emission reaches 8.94 g/kWh, while at 2000 bar–0.67 g/kWh. It is worth mentioning that at 1000 and 1500 bar, NH_3 emissions were 1.51 and 1.05 g/kWh, respectively. Between 1000 and 2000 bar, the difference in NH_3 emissions is not significant, which can be attributed to a negligible difference in T_{max} between 1731 and 1779 K. In conclusion, fuel injection pressure has a significant effect on combustion efficiency, which in turn affects unburnt NH_3 emissions.

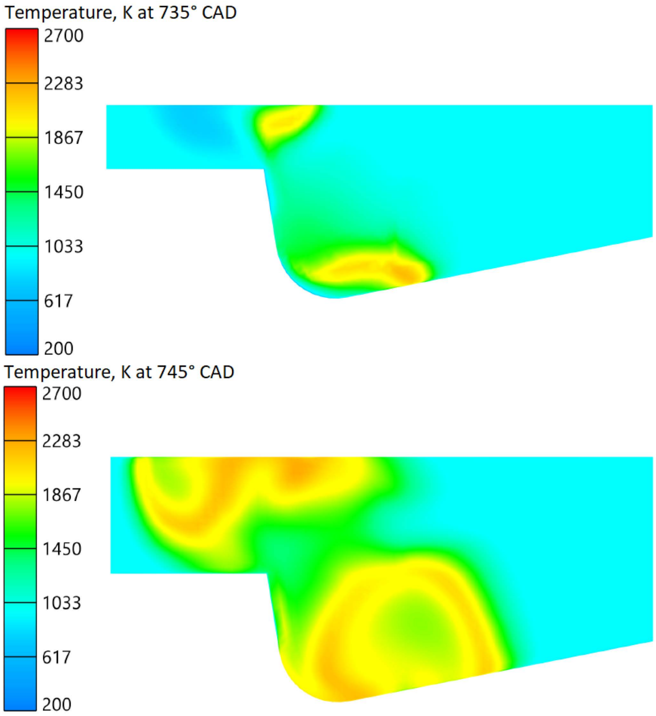

(**a**) P_{inj}—500 bar

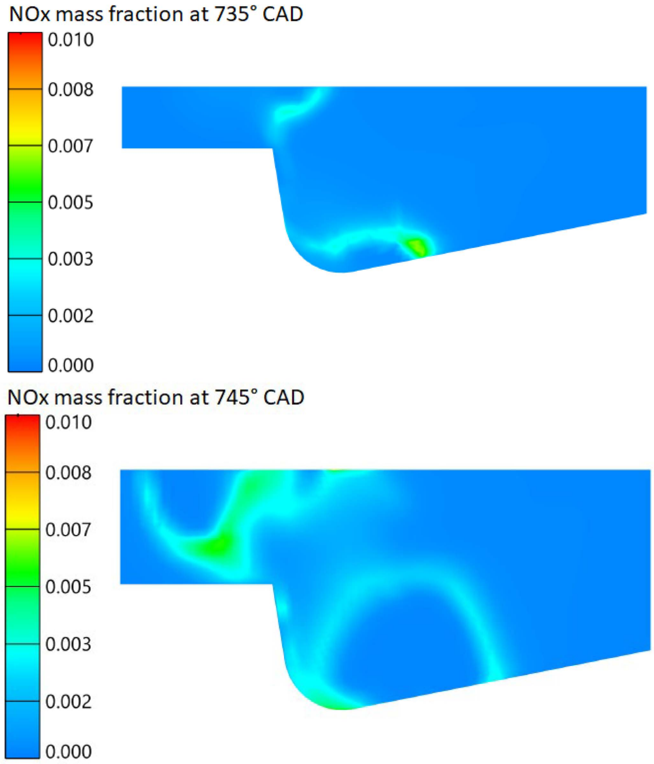

(**d**) P_{inj}—500 bar

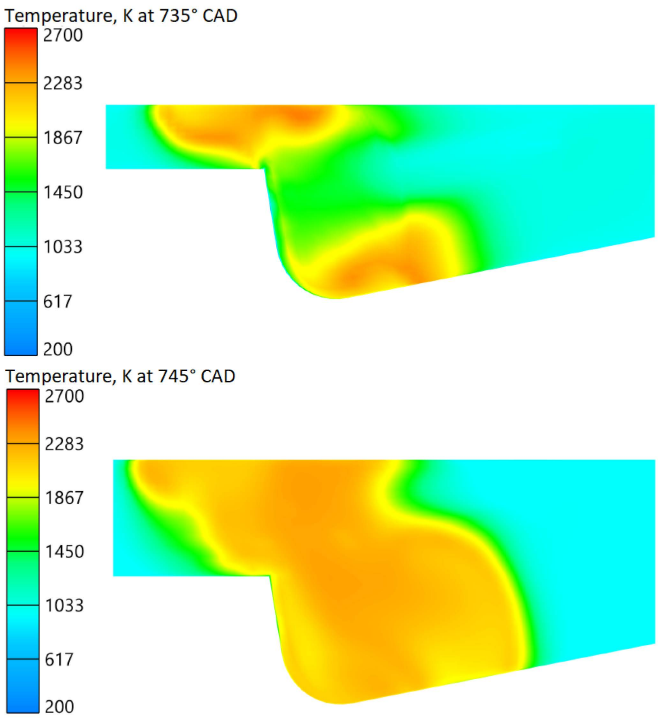

(**b**) P_{inj}—1000 bar

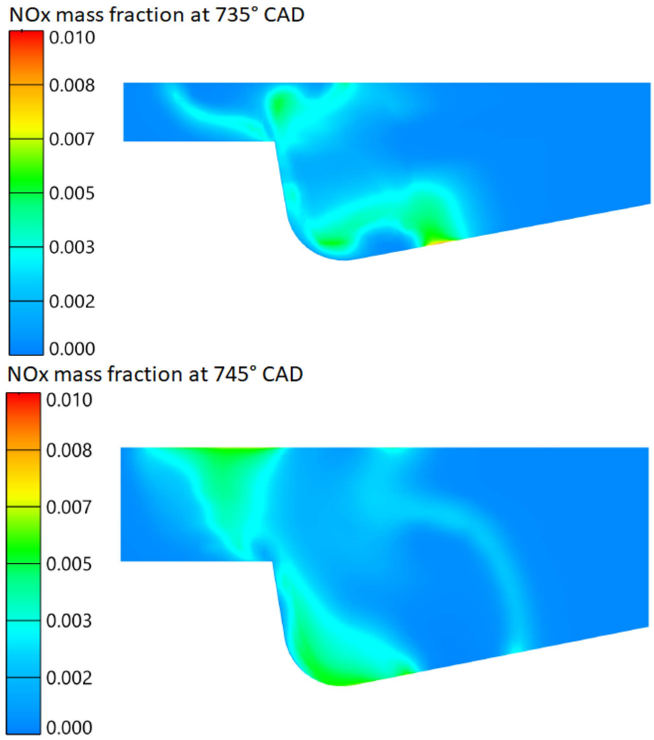

(**e**) P_{inj}—1000 bar

Figure 9. *Cont.*

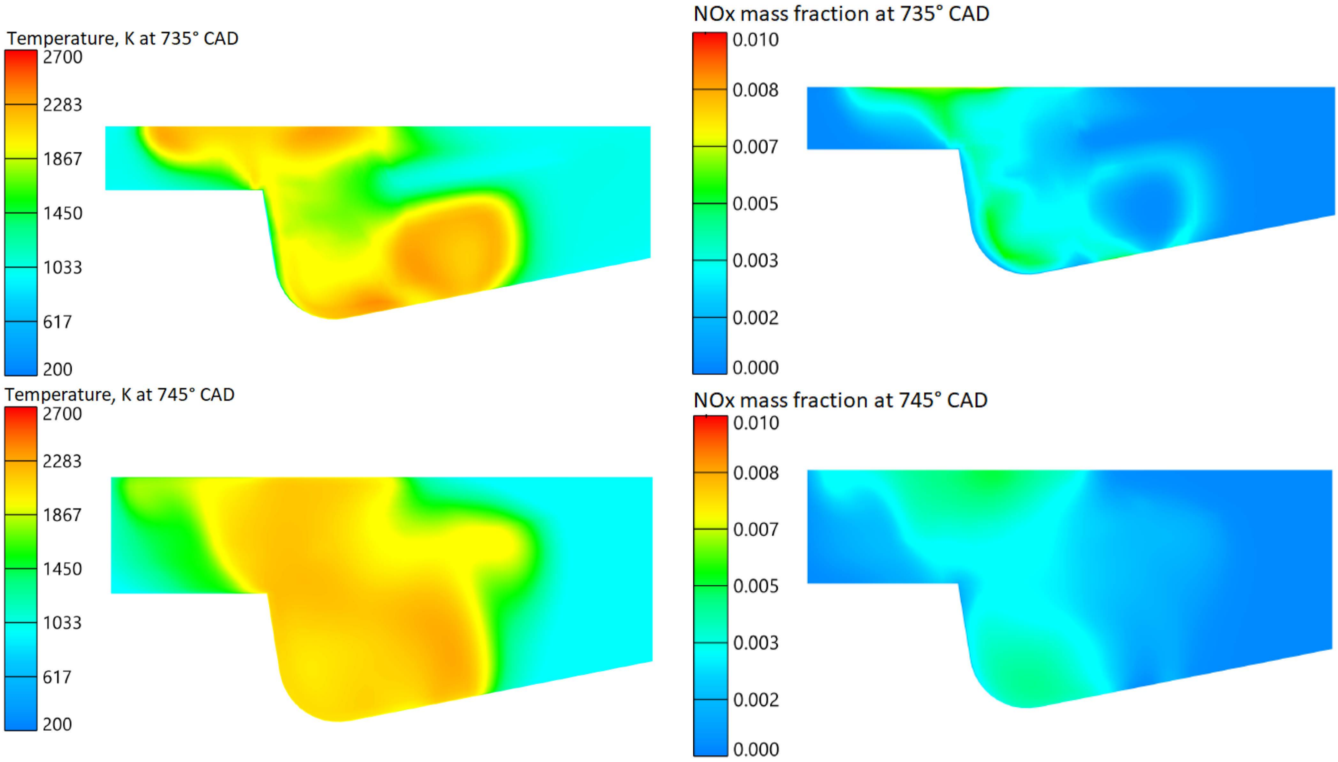

(**c**) P_{inj}—2000 bar (**f**) P_{inj}—2000 bar

Figure 9. Comparison of NO_x cyclic mass fraction in combustion chamber with temperature fields at 735° and 745° CAD at 500, 1000, and 2000 ammonia injection pressure. (**a**–**c**) Temperature; (**d**–**f**) NO_x mass fraction.

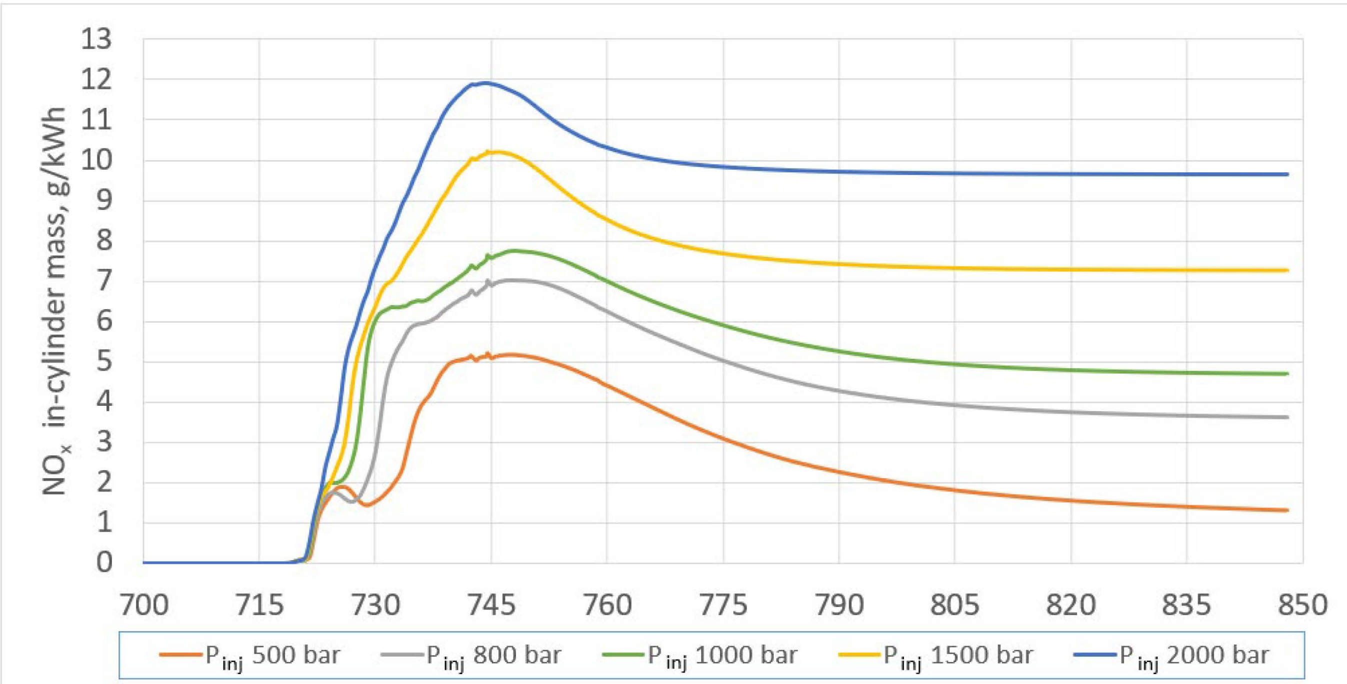

Figure 10. Comparison of NO_x formation during the combustion cycle at different ammonia injection pressures.

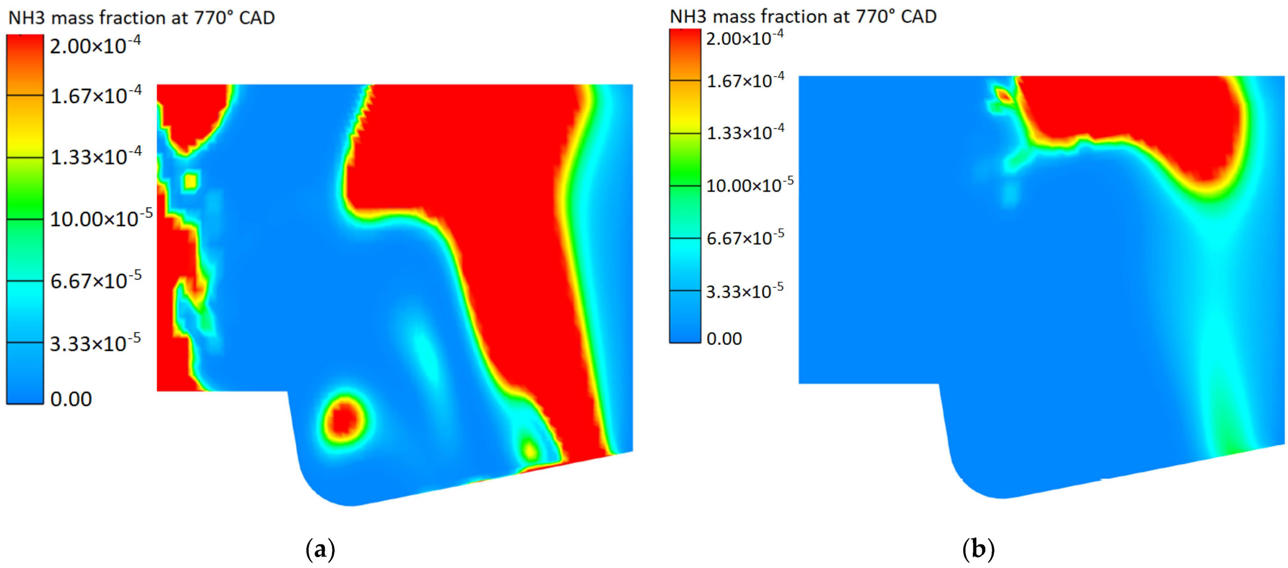

Figure 11. Comparison of the NH_3 cyclic mass fraction in the combustion chamber at 770° CAD. (**a**) Ammonia injection pressure 500 bar; (**b**) ammonia injection pressure 2000 bar.

In terms of GHG emissions when using ammonia in DE, N_2O has the biggest impact according to CO_2 potential (GHG = 273 × N_2O + 29.8 × CH_4 + CO_2) (Figure 12). At 2000 bar injection pressure at high combustion temperature outside the N_2O formation field, GHG emissions are lowest, 195 g/kWh, while at 500 bar–490 g/kWh. In all cases, using ammonia can reduce GHG emissions, as the D100 combustion cycle GHG is 684 g/kWh. However, GHG reduction in the reverse direction increases NO_x emissions. On the other hand, NO_x reduction leads to higher unburnt NH_3 emissions. Therefore, balance between main GHG (N_2O), NO_x, and NH_3 emissions should be selected.

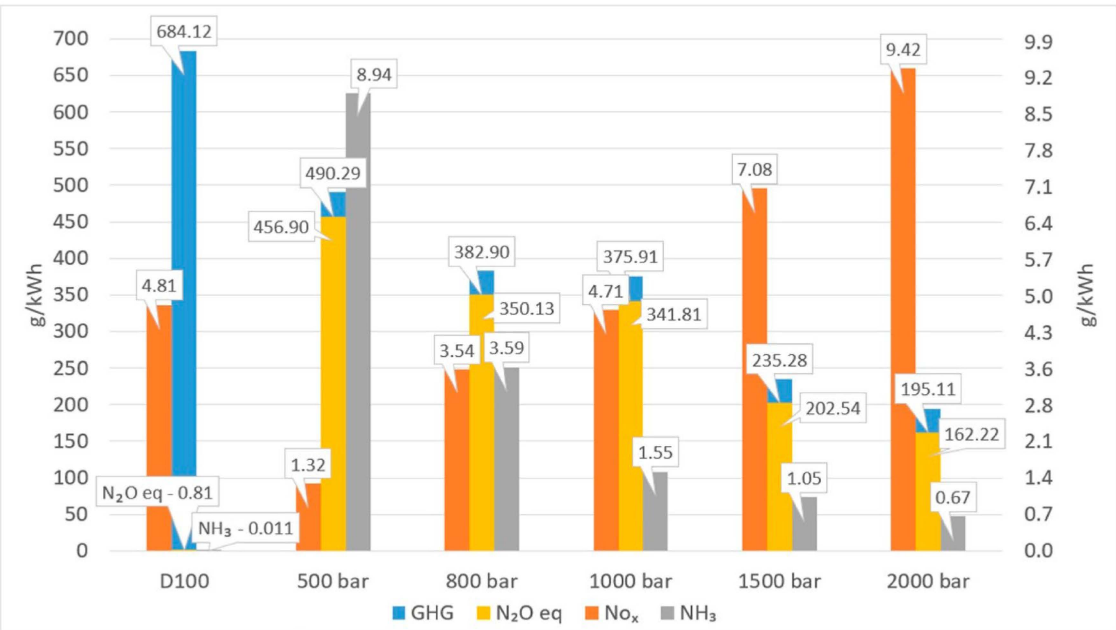

Figure 12. Comparison of emissions (GHG, N_2O eq, NO_x, and NH_3) formation during the combustion cycle at different ammonia injection pressures.

Summarizing the results of ammonia injection pressure dependence on combustion cycle parameters and exhaust gas emissions, the optimal injection pressure due to P_{max} and T_{max} design limitation is 800–1000 bar. In addition, ITE at these injection pressures compared to the 2000 bar was practically unchanged. In terms of toxic emissions, the balance between GHG, NO_x, and NH_3 is also at 800–1000 bar injection pressure. At 1000 bar injection pressure, GHG emission is 4.5% lower and NH_3 is 137% lower, although NO_x is 30% higher compared to 800 bar injection pressure. Therefore, the optimal ammonia injection pressure for the research object is 1000 bar, considering changes in combustion cycle parameters.

Summarized research main combustion cycle parameters and exhaust gas emission values are given in Table 5.

Table 5. Simulation results of ammonia injection pressure variations.

Parameter	D100 (P_{inj} 500 bar)	P_{inj} 500 bar	P_{inj} 800 bar	P_{inj} 1000 bar	P_{inj} 1500 bar	P_{inj} 2000 bar
T_{max}	1566.00	1540	1668	1731	1751	1779
P_{max}	159.60	132.18	161.34	175.38	185.46	193.78
IMEP	17.24	17.86	18.29	18.28	18.36	18.30
ITE	0.407	0.416	0.426	0.426	0.428	0.426
BSFC(D)	208.04	11.13	10.87	10.88	10.83	10.87
BSFC(NH_3)	-	434.84	424.68	425.01	422.97	424.53
P_i (complete engine)	4314.37	4191.17	4291.45	4288.09	4308.83	4293.00
CO_2	563.95	33.32	32.72	33.24	32.72	32.88
N_2O	0.0030	1.67	1.28	1.22	0.74	0.59
CH_4	4.01	0.00249	0.00132	0.000505	0.00037	0.00023
GHG	684.12	490.29	382.90	366.60	235.28	195.11
NO_x	4.81	1.32	3.54	4.59	7.08	9.42
NH_3	0.011	8.94	3.59	1.51	1.05	0.67

4. Conclusions

To optimize the dual ammonia and diesel fuel combustion cycle, combustion cycle parameters and exhaust gas emissions optimization strategy was chosen based on DE development trends and intensification of ammonia injection using high-pressure injection to reduce combustion duration. GHG emissions in CO_2 equivalent were reduced by 24% when ammonia injection pressure was increased from 500 bar to 1000 bar. For comparison, GHG emissions were also reduced by 45% compared to the diesel combustion cycle. Based on this research's results, detailed changes in the combustion cycle are characterized by the following:

- An ammonia injection pressure increase from 500 bar to 2000 bar reduces ammonia induction period by 28% from 18° CAD to 13° CAD. Correspondingly, ammonia ignition delay after pilot diesel fuel combustion shortens from 6° CAD to 1° CAD. As a result, at injection pressure 500 bar, a transformation of double-phase combustion characteristic into single-phase at 800–2000 bar injection pressure leads to structural changes in the combustion cycle parameters and exhaust gas emissions.
- At 500 bar ammonia injection pressure, the long induction period and double-phase combustion characteristic results in a long ~60° CAD combustion duration (D100—90° CAD). Meanwhile, by gradually increasing the injection pressure of over 800 bar and approaching the single-phase combustion characteristic, the combustion duration is reduced to 20–30° CAD.
- Due to the long combustion duration at 500 bar ammonia injection pressure, 2.4% lower ITE was reached than compared to higher injection pressure due to higher heat balance losses through the cooling–exhaust system. At 500 bar, ITE = 41.6%, while at 800–2000 bar, ITE = 42.6–42.8%. Therefore, at ammonia injection pressure above 800 bar, 4.6% higher ITE was reached compared to the D100 combustion cycle.
- An injection pressure increase over 800 bar leads to a higher P_{max} and T_{max} than the D100 combustion cycle. P_{max} increases from 161 bar to 194 bar by increasing injection pressure from 800 bar to 2000 bar, while T_{max} increases from 1670 K to 1780 K. For comparison, D100 P_{max}–160 bar, and T_{max}–1565 K.

- GHG emissions decreased from 684 g/kWh at D100 to 490 g/kWh–195 g/kWh at ammonia injection pressure 500–2000 bar. GHG emissions from dual ammonia–diesel fuel combustion mainly did not depend on CO_2 as in the D100 case, but depended on N_2O, whose formation is associated with N atoms in fuel. The possibility to reduce N_2O emissions is associated with the increase of combustion chamber temperature.
- Unburnt NH_3 reached maximum of 8.95 g/kWh at 500 bar injection pressure, which indicated poor combustion efficiency. Gradually increasing injection pressure from 800 bar to 2000 bar reduced NH_3 emissions from 3.60 g/kWh to 0.65 g/kWh, respectively.
- NO_x emissions can be reduced from 4.81 g/kWh at D100 to 1.32 g/kWh at ammonia injection pressure 500 bar. However, at the same time, it can increase to 9.42 g/kWh at 2000 bar injection pressure. NO_x formation depends on N atoms in fuel, but at the same time depends on combustion chamber temperature. The lower NO_x levels at 500 bar ammonia injection pressure than D100 can be explained by the deNO_x process. On the other hand, higher NO_x levels at high ammonia injection pressures are directly linked to thermal NO_x formation due to increased combustion chamber temperature.

In conclusion, when optimizing the combustion cycle of dual ammonia and diesel fuel, it is rational to achieve short, single-phase combustion, but within permissible P_{max} and T_{max} boundaries, ensuring the engine reliability factor compared to D100. In parallel, when selecting ammonia injection pressure, a compromise of GHG, unburnt NH_3, and NO_x emissions must be ensured to maintain optimal balance between these harmful substances. As a result, the optimal ammonia injection pressure for medium-speed, four-stroke Wartsila 6L46 marine diesel engine is 1000 bar. The next stage of ammonia combustion cycle optimization research will be associated with the optimization of pilot diesel and ammonia injection phases.

Author Contributions: Conceptualization, S.L.; Methodology, M.D.; Software, M.D.; Validation, M.D.; Formal analysis, M.D.; Data curation, S.L.; Writing – original draft, M.D.; Writing – review & editing, S.L.; Supervision, S.L. All authors have read and agreed to the published version of the manuscript.

Funding: The project was financed by Research Council of Lithuania and the Ministry of Education, Science and Sport Lithuania (Contract No. S-A-UEI-23-9).

Institutional Review Board Statement: Not applicable.

Informed Consent Statement: Not applicable.

Data Availability Statement: Data are contained within the article.

Acknowledgments: The authors thank AVL company for their long-term cooperation with Klaipeda University for providing AVL FIRE simulation software used in the PhD study program in maritime transport decarbonization research. Exceptional thanks to AVL FIRE personnel for sharing limited accessibility to the ammonia gas reaction mechanism, consultation, and professional advice.

Conflicts of Interest: The authors declare no conflict of interest.

Abbreviations

B/S	cylinder bore, stroke;
BSFC	specific fuel consumption;
CAD	crank angle degrees;
CH_4	methane;
CO_2	carbon dioxide;
D100	100% diesel fuel;
D5/A95	mixture of 5% diesel and 95% ammonia fuel;
DE	diesel engine;
EEDI	Energy Efficiency Design Index;
EEXI	Efficiency Existing Ship Index;
EU	European Union;

GHG	greenhouse gases;
GT	gross tonnage;
HPDF	high-pressure dual-fuel strategy;
HRC	heat release characteristic;
IMEP	indicated mean indicative pressure;
IMO	International Maritime Organization;
ITE	indicative thermal efficiency;
LNG	liquified natural gas;
LPDF	low-pressure dual-fuel strategy;
MM	mathematical model;
N_2O	dinitrogen oxide;
NH_3	ammonia;
NO_x	nitrous oxides;
PM	particulate matter;
SCR	selective catalytic reduction;
TDC	top dead center;
Symbols	
H_u	fuel calorific value (kJ/kg);
m_f	hourly fuel consumption (kg/h);
n	cylinder number (-);
N	engine speed (RPM);
P_i	indicated power (kW);
P_{inj}	ammonia injection pressure (bar);
P_k	cylinder pressure reading (bar);
P_{max}	maximum cycle pressure (bar);
T_{max}	maximum cycle temperature (K);
T	temperature (K);
V_{cyl}	cylinder volume (m^3);
V_k	cylinder volume corresponding to P_k (m^3);
z	coefficient (z = 1 for 2-stroke engines, z = 2 for 4-stroke engines (-);
θ_0	crank angle degree value (-);
θ_f	crank angle degree value (-);

References

1. SEC (2021) 562 Final. Regulation of the European Parliament and of the Council on the Use of Renewable and Low-Carbon Fuels in Maritime Transport and Amending Directive 2009/16/EC. Available online: https://eur-lex.europa.eu/legal-content/EN/ALL/?uri=COM:2021:562:FIN (accessed on 3 January 2024).
2. International Maritime Organization. Energy Efficiency Measures. Available online: https://www.imo.org/en/OurWork/Environment/Pages/Technical-and-Operational-Measures.aspx (accessed on 3 January 2024).
3. International Maritime Organization. Rules on Ship Carbon Intensity and Rating System Enter into Force. Available online: https://www.imo.org/en/MediaCentre/PressBriefings/pages/CII-and-EEXI-entry-into-force.aspx (accessed on 3 January 2024).
4. International Maritime Organization. Annex 15, Resolution MEPC.377(80). 2023 Strategy on Reduction of GHG Emissions from Ships. Available online: https://wwwcdn.imo.org/localresources/en/OurWork/Environment/Documents/annex/MEPC%2080/Annex%2015.pdf (accessed on 5 January 2024).
5. DNV Report. Maritime Forecast to 2050. Available online: https://www.dnv.com/maritime/publications/maritime-forecast-2023/index.html (accessed on 5 January 2024).
6. UNCTAD. Review of Maritime Transport. Available online: https://unctad.org/system/files/official-document/rmt2021_en_0.pdf (accessed on 6 January 2024).
7. DNV Group. Maritime Forecast to 2050. Available online: https://www.dnv.com/maritime/publications/maritime-forecast-2022/download-the-report.html (accessed on 6 January 2024).
8. Aziz, M.; Wijayanta, A.T.; Nandiyanto, A.B.D. Ammonia as Effective Hydrogen Storage: A Review on Production, Storage and Utilization. *Energies* **2020**, *13*, 3062. [CrossRef]
9. Reiter, A.J.; Kong, S.C. Combustion and emissions characteristics of compression-ignition engine using dual ammonia-diesel fuel. *Fuel* **2011**, *90*, 87–97. [CrossRef]
10. Ryu, K.; Zacharakis-Jutz, G.E.; Kong, S.C. Performance characteristics of compression-ignition engine using high concentration of ammonia mixed with dimethyl ether. *Appl. Energy* **2014**, *113*, 488–499. [CrossRef]

11. Dimitriou, P.; Javaid, R. A review of ammonia as a compression ignition engine fuel. *Int. J. Hydrog. Energy* **2020**, *45*, 7098–7118. [CrossRef]
12. Nadimi, E.; Przybyła, G.; Lewandowski, M.T.; Adamczyk, W. Effects of ammonia on combustion, emissions, and performance of the ammonia/diesel dual-fuel compression ignition engine. *J. Energy Inst.* **2023**, *107*, 101158. [CrossRef]
13. Li, T.; Zhou, X.; Wang, N.; Wang, X.; Chen, R.; Li, S. A comparison between low and high-pressure injection dual-fuel modes of diesel-pilot-ignition ammonia combustion engines. *J. Energy Inst.* **2022**, *102*, 362–373. [CrossRef]
14. Scharl, V.; Sattelmayer, T. Ignition and combustion characteristics of diesel piloted ammonia injections. *Fuel Commun.* **2022**, *11*, 100068. [CrossRef]
15. Yousefi, A.; Guo, H.; Dev, S.; Liko, B.; Lafrance, S. Effects of ammonia energy fraction and diesel injection timing on combustion and emissions of an ammonia/diesel dual-fuel engine. *Fuel* **2022**, *314*, 122723. [CrossRef]
16. Li, T.; Zhou, X.; Wang, N.; Wang, X.; Chen, R.; Li, S. Pilot diesel-ignited ammonia dual fuel low-speed marine engines: A comparative analysis of ammonia premixed and high-pressure spray combustion modes with CFD simulation. *Renew. Sustain. Energy Rev.* **2023**, *173*, 113108.
17. Lyon, R.K. The chemistry of the thermal DeNOx process: A review of the thechnology's possible application to control of NOx from diesel engines. In Proceedings of the 7th Diesel Engine Emissions Reduction (DEER) Workshop 2001, Portsmouth, VA, USA, 5–9 August 2001.
18. Zinner, K. Results of real cycle calculations about the possibilities of influencing the efficiency of diesel engines. *MTZ* **1970**, *31*, 243–246.
19. Stechkin, B.S. On the efficiency of an ideal fast combustion cycle at a finite rate of heat release. Theory, design, calculation and testing of internal combustion engines. *Proc. Lab. Engines USSR Acad. Sci.* **1960**, 61–67.
20. Semenov, B.N.; Ivanchenko, N.N. Problems of increasing the fuel efficiency of diesel engines and ways to solve them. *Engine Engineering.* **1990**, *11*, 3–7.
21. Kruggel, O. Progress in the combustion technology of high performance diesel engines toward reduction of exhaust emissions without reduction of operation economy. In Proceedings of the Baden–Wurttemberg Technology Conference, Oslo, Norway, 8 February 1989; p. 14.
22. Schulte, H.; Duernholz, M.; Wuebbeke, K. The Contribution of the fuel injection system to meeting future demands on truck diesel engines. *SAE Trans.* **1990**, *99*, 157–162.
23. MTU, Deutsche Aerospace. *Series 396 Engines*; VTS 05076 (520 E); MTU, Deutsche Aerospace: Munich, Germany, 1990; 22p.
24. Shundoh, S.; Kakegawa, T.; Tsujimura, K.; Kobayashi, S. The effect of injection parameters and swirl on diesel combustion with high pressure fuel injection. *SAE Trans.* **1991**, *100*, 793–805.
25. Stas, M.; Wajand, J.; Bestimmung, d.V. Parameters for the two-phase combustion process in direct injection diesel engines. *MTZ Mot.* **1988**, *49*, 289–293.
26. Kruggel, O. Studies on nitrogen oxide reduction in high-speed large diesel engines. *MTZ Mot.* **1988**, *49*, 22–29.
27. Kakaee, A.H.; Rahnama, P.; Paykani, A. Influence of fuel composition on combustion and emissions characteristics of natural gas/diesel RCCI engine. *J. Nat. Gas Sci. Eng.* **2015**, *25*, 58–65. [CrossRef]
28. Yang, B.; Xi, C.; Wei, X.; Zeng, K.; Lai, M.C. Parametric investigation of natural gas port injection and diesel pilot injection on the combustion and emissions of a turbocharged common rail dual-fuel engine at low load. *Appl. Energy* **2015**, *143*, 130–137. [CrossRef]
29. Gatts, T.; Liu, S.; Liew, C.; Ralston, B.; Bell, C.; Li, H. An experimental investigation of incomplete combustion of gaseous fuels of a heavy-duty diesel engine supplemented with hydrogen and natural gas. *Int. J. Hydrog. Energy* **2012**, *37*, 7848–7859. [CrossRef]
30. Lebedevas, S.; Raslavičius, L.; Drazdauskas, M. Comprehensive correlation for the prediction of the heat release characteristics of diesel/CNG mixtures in a single-zone combustion model. *Sustainability* **2023**, *15*, 3722. [CrossRef]
31. Lebedevas, S.; Raslavičius, L.; Rapalis, P. Simulation of microalgae oil spray characteristics for mechanical fuel injection and CRDI systems. *Biomass Convers. Biorefinery* **2022**, 1–16. [CrossRef]
32. Lebedevas, S.; Čepaitis, T. Parametric analysis of the combustion cycle of a diesel engine for operation on natural gas. *Sustainability* **2021**, *13*, 2773. [CrossRef]
33. Lebedevas, S.; Čepaitis, T. Research of organic rankine cycle energy characteristics at operating modes of marine diesel engine. *J. Mar. Sci. Eng.* **2021**, *9*, 1049. [CrossRef]
34. Woodyard, D. Medium speed engines—Introduction. In *Marine Diesel Engines*; Elsevier: Amsterdam, The Netherlands, 2004; pp. 498–516.
35. Molland, A.F. Marine engines and auxiliary machinery. In *The Maritime Engineering Reference Book*; Elsevier: Amsterdam, The Netherlands, 2008; pp. 344–482.
36. Bergen B33:45L Marine Diesel Engine Specification. Available online: https://www.bergenengines.com/engines/b33-45l/ (accessed on 15 January 2024).
37. MAN L48/60CR Marine Diesel Engine Specification. Available online: https://www.man-es.com/marine/products/four-stroke-engines/propulsion (accessed on 15 January 2024).
38. Wartsila 46F Marine Diesel Engine Specification. Available online: https://www.wartsila.com/marine/products/engines-and-generating-sets/diesel-engines/wartsila-46f (accessed on 15 January 2024).

39. Glarborg, P.; Miller, J.A.; Ruscic, B.; Klippenstein, S.J. Modeling nitrogen chemistry in combustion. *Prog. Energy Combust. Sci.* **2018**, *67*, 31–68. [CrossRef]
40. Dukowicz, J.K. A Particle-fluid numerical model for liquid sprays. *J. Comput. Phys.* **1980**, *35*, 229–253. [CrossRef]
41. Schiller, L.; Naumann, A. A Drag Coefficient Correlation. *VDI Ztg.* **1933**, *77*, 318–320.
42. Abramzon, B.; Sirignano, W.A. Droplet vaporization model for spray combustion calculations. In Proceedings of the AIAA 26th Aerospace Sciences Meeting, Reno, NV, USA, 11–14 January 1988.
43. Javaherian, H.; Haskara, I.; Dagci, O.H. Technique for Calculating a High-Precision IMEP Using a Low-Resolution Coder and an Indirect Integration. Process Patent DE102011011485A1, 22 March 2012.
44. Mollenhauer, K.; Tschöke, H. *Handbook of Diesel Engines*; Springer: Berlin/Heidelberg, Germany, 2010; pp. 8–24.
45. Mondal, P.K.; Mandal, B.K. Effect of fuel injection pressure on the performances of a CI engine using water-emulsified diesel (WED) as a fuel. *Energy Sustain. Soc.* **2024**, *14*, 12. [CrossRef]
46. Geng, L.; Wang, Y.; Wang, Y.; Li, H. Effect of the injection pressure and orifice diameter on the spray characteristics of biodiesel. *J. Traffic Transp. Eng.* **2020**, *7*, 331–339. [CrossRef]
47. Hebbar, G.S. NOx from diesel engine emission and control strategies—A review. *Int. J. Mech. Eng. Eobotics Res.* **2014**, *3*, 471.